PERGAMON

International Journal of Solids and Structures 38 (2001) 5453–5464

INTERNATIONAL JOURNAL OF SOLIDS and STRUCTURES

www.elsevier.com/locate/ijsolstr

# Experimental study of spall-fracture zone

A.P. Rybakov

*Perm State Technical University, P.O. Box 1864, Perm' 101, 614101 Perm, Russian Federation*

Received 16 March 1999; in revised form 20 July 2000

**Abstract**

The experimental results of spall damage investigation of two metals under sliding detonation are presented. The damage distribution across specimen thickness has been studied by experiments and described by the proposed kinetics. Experimental results were confirmed by data from other authors. Some aspects of spall phenomenon are also discussed here. © 2001 Elsevier Science Ltd. All rights reserved.

*Keywords:* Spall-fracture zone; Damage distribution; Kinetics

## 1. Introduction

Under spallation we observe an unstationary shock wave with pressure decrease behind the shock wave front. When the wave has reached the free surface of a specimen, a rarefaction wave is reflected back into the body. The shock and rarefaction wave interaction results in spallation. The substance layer closely adjacent to the free surface of the specimen separates and flies apart from the main part of the body. The goal of the paper is mainly to present new experimental results of spall-fracture zone. Investigations in the world of scientific literature reveal that, there are no experimental data of systematical analysis of distribution of the damage along thickness of specimen under loading. This paper gives an answer to this question in one partial case.

People have been modelling spallation phenomenon for a long time. Among different theories on spallation, the acoustic theory proposed by Rinehart and Pearson (1954) and developed by Broberg (1960) and in Altshuler et al. (1966) is the simplest. According to this theory for a certain amount of time the tensile stress is constant on each plane parallel to the free surface. The magnitude of this stress equals zero on the free surface and increases to its maximum with a distance increase from the surface. The break of continuity is located in a narrow thin plane area at some distance from the free surface with its maximum in the vicinity of the plane, where the co-ordinate $x_\delta$ is the hypothetical plane of a spall (Fig. 1). In reality, there is a certain region of damage localization. The spalled layer of thick $\delta$ is located between the plane $x\delta$ and the free surface. Experiments show that the break of continuity is negligible outside this narrow region.

*E-mail address:* zakamsk@pstu.c.a.ru (A.P. Rybakov).

0020-7683/01/$ - see front matter 
PII: S0020-7683(00)00301-2

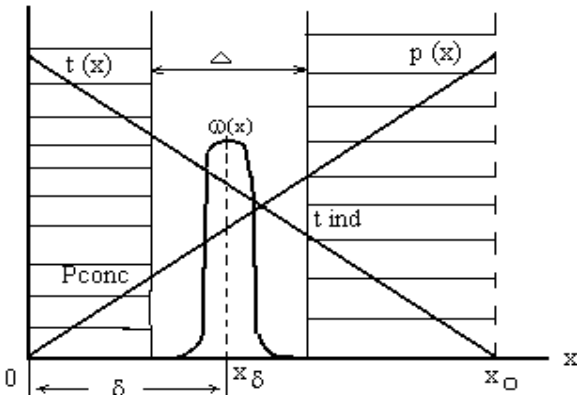


Fig. 1. The tensile stress $P(x)$, tension time $t(x)$ and damage factor $\omega(x)$ distribution along the coordinate $x$: $x = 0$ is the free surface coordinate; $x_\delta$ is the coordinate for hypothetical plane of spall; $x_0$ is the coordinate where the shock and reflected rarefaction waves diverge; $(0–x_0)$ is the region of tensile stresses.

Some recent works (see e.g. Curran et al., 1987; Grady, 1988; Beliaev et al., 1989; Eftis et al., 1991; Novikov, 1999; Kanel et al., 1999) give results of investigation of a damage region structure and study some other short-duration processes in this region. Some other techniques of spallation analysis e.g. macroscopic one, are also relevant. Microscopic technique of spall investigation has been chosen in the present paper. Of course, the acoustical model of spalling is rather primitive. Furthermore, it may be that the estimated stress histories apparently do not account for the stress relaxation that occurs during the evolution of damage, thereby changing both the tensile stress amplitude and duration. But, this model gives enough satisfactory picture of the macroscopic aspects of the problem (see e.g. Rinehart and Pearson, 1954; Broberg, 1960; Altshuler et al., 1966; Kanel et al., 1999; and Fig. 6 of this paper). Data in Fig. 6 have been obtained as by means of acoustical model (Fig. 6a and b) and so in the framework of model for non-equlibrium static thermodynamics. Last model is one that is certainly advantageous in comparison with the other publications.

The present paper, has a secondary goal: to test an engineering model for predicting the amount of spall in impulsively loaded specimens. This model also serves (i) to express hypothesis about the analogy of the spall process to the kinetics of the explosive reaction, (ii) to validate an induction time aspect. Spall damage as a fragmentation problem has been investigated in sufficient detail for the plane one-dimensional loading (among recent works on this subject see e.g. Novikov, 1985; 1999; Kanel et al., 1999). The information on spall damage of specimens in non-one-dimensional conditions is given here to provide better understanding of the phenomenon under consideration. This work consists of several parts.

## 2. Explosion experiments

The shock wave experiments were performed using a plane specimen covered by a sheet explosive charge. The specimen's dimensions were $80 \times 120$ mm$^2$ with variation. The sheet charge was 2 mm thick. Materials studied were steel $C_T3$ and aluminium alloy D16. Mechanical properties of these materials are given in Table 1. The specimens tested did not have any treatment before the experiment. The specimens were 4, 5, 7, 12, 16 mm thick for steel and 2, 3, 4, 6, 10 mm thick for aluminium alloy. The specimen sizes were taken to prevent the influence of side rarefaction on the central part of specimens. The explosive charge had the following parameters density $1.67 \times 10^3$ kg/m$^3$, detonation velocity 7.4 km/s, heat of explosion is $6.4 \times 10^6$ J/kg.

Table 1
Mechanical properties of materials

| Material | Percentage of elements (%) | | | | Tensile breaking point (MPa) | Fluidity point (MPa) | Conventional fluidity under point at residual deformation of 0.2% (MPa) | Relative lengthening under break (%) | Hardness (Hb) |
|---|---|---|---|---|---|---|---|---|---|
| | C | Mn | Cu | Mg | | | | | |
| Steel $C_T3$ | 0.14–0.22 | 0.3–0.65 | | | 380–490 | $\geqslant 210$ | | 23 | 180 |
| Aluminium alloy D16 | | 0.3–0.9 | 3.8–4.9 | 1.2–1.8 | 440 | | 330 | 18 | 1050 |

The charge was initiated simultaneously along a line at all its points. This line was normal to the direction of detonation motion. The sliding detonation wave propagated over the charge (Fig. 2) and produced in the specimen an oblique damping shock wave, which reached the free surface. After that, a reflected rarefaction wave returned back into the specimen. A layer of ultimate thickness was turned and flew apart from the main part of the specimen. Such a phenomenon including a separated layer itself is called a spall.

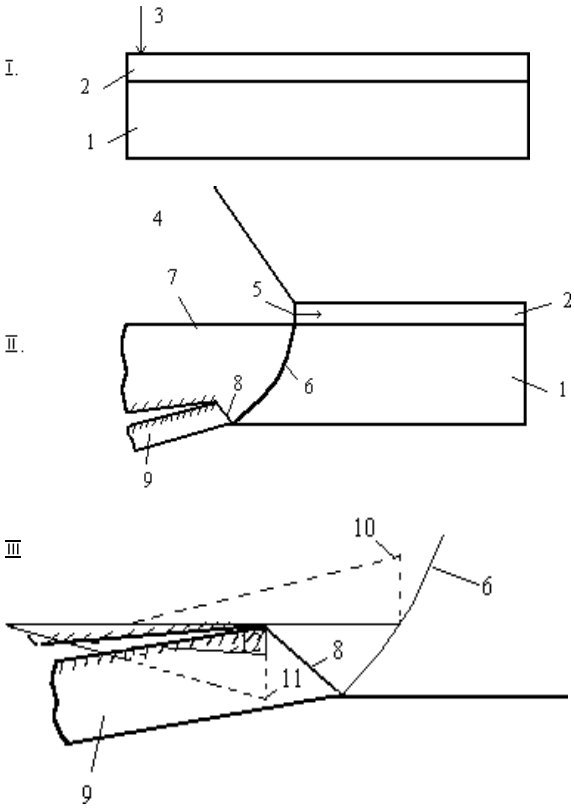


Fig. 2. Experimental arrangement I – original state; II – state after the initiation of detonation; III – rupture region. 1 – specimens with thickness of $H$: 2 – sheet explosive charge with thickness of $h$; 3 – initiating unit; 4 – explosion products; 5 – detonation wave front; 6 – damping shock wave; 7 – explosion products-shocked material boundary; 8 – reflected rarefaction wave; 9 – spalled layer; 10 – pulse of compression wave; 11 – reflected pulse of rarefaction wave; 12 – tension pulse in the rupture section.

In the experiments, the shock-loaded specimens and separated layers were trapped. Steel specimens demonstrated partial or full rupture. The main crack was formed in the specimens 16 mm thick but no complete separation of the specimen into multiple parts took place. All other specimens demonstrated complete separation into the main and spalled parts. Two spall layers were observed in specimens of 5 mm thick. Their rupture surfaces were almost smooth whereas those of the other specimens were porous and scaled. As for aluminium specimens, their rupture surfaces were also porous and scaled. The scales sizes increased with the specimen thickness. No rupture was observed in the specimens of 2 and 3 mm thick.

## 3. Metallographical experiments

Metallographical investigations of the specimens tested were made. The shock loaded specimens were cut along the centre line and across it. The specimen cut cross-section was parallel to the direction of detonation wave propagation in the first case, and perpendicular to it in the second case. The cut pieces were pressed into plastic shells and then polished. The polished specimens were investigated by a metallographical microscope.

A zone, 2 mm wide along the height micro cross-section was studied at a 200× magnification. The pictures of damage distribution along thickness are presented in Fig. 3. These pictures have been obtained from experimental micrographs for aluminium alloy D16 specimens of 4 and 6 mm thick. Cracks of 2.5 μm wide and larger were seen. The picture of micro-cross-section was separated into zones parallel to the loaded surface. The total area occupied by cracks, pores and other continuous damage was calculated for each micro-cross-zone. Then the ratio $\omega$ of the total area of continuous damage to the area of a chosen zone was calculated. The magnitudes of $\omega$ are equal both for 'parallel' sections, and for 'perpendicular' sections. Therefore, the ratio $\omega$ was called damage factor. Further, $\omega$ has been interpreted as ratio of volume of voids to all volume of region under consideration. In other words, the damage factor is fractional voids volume in given volume. Damage distribution was defined as a function of coordinate along specimen thickness.

The distributions such obtained are given in Figs. 4 and 5 for sections perpendicular to the direction of detonation wave motion. Some experimental results are given in Table 2, which contains such parameters as the spalled layer thickness, the width of fracture zone and the width the zone of complete fracture.

## 4. Estimation of state parameters of zone under consideration

The usual way to evaluate the shock wave parameters under impulse loading created by an explosion of high explosives has been to describe them hydrodynamically, whereas in condition of shock wave damping it is reasonable to use the stress-wave approximation. However, the difference in magnitudes of spall parameters obtained in both cases is rather small. For example, the difference in spall strength is less than 10% (as it affirmed by Zlatin et al., 1984). The analysis of the above is given in Rybakov (1996a,b). Therefore, further we shall use the hydrodynamics approximation, namely, the acoustic model of spallation.

From ($P$–$\theta$) diagram proposed by Rybakov (1991) and then developed in Rybakov and Rybakov (1993) and Rybakov (1993a,b) the loading pulse parameters at the contact boundary were determined. The pressure amplitude of loading pulse at the contact boundary between the detonation products and specimen material was determined as follows. The magnitudes of pressure ($P$) and angle ($\theta$) must be equal for the detonation products and loaded material. The flow in detonation products is Prandtl–Meyer's flow. The flow in specimens is a flowing around a concave angle formed by the front of oblique shock wave. The following equations were written:

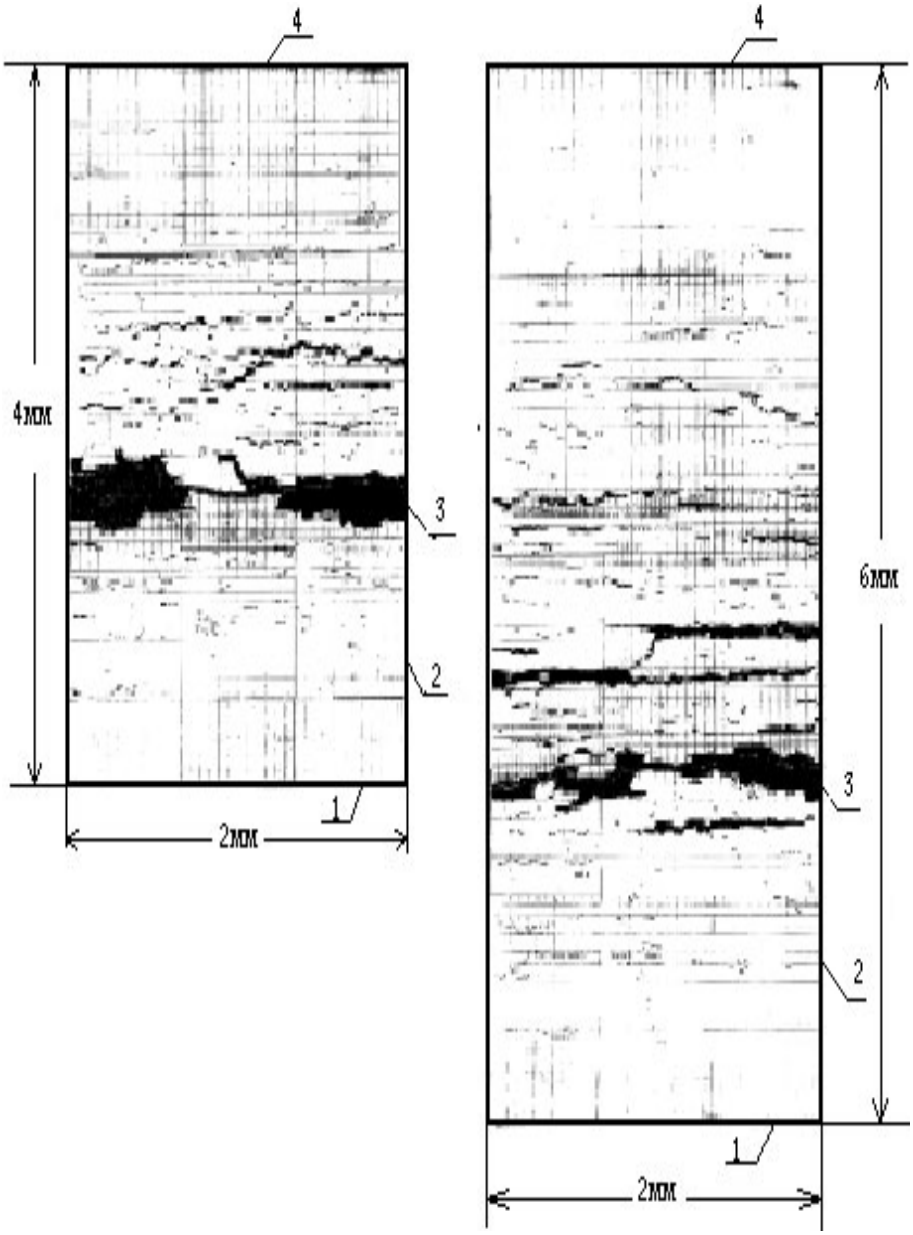


Fig. 3. Micrographs-pictures of distribution of damage along thickness of specimens from aluminium alloy. 1 – free surface; 2 – spalled layer; 3 – dispersed material of complete fracture zone; 4 – loaded surface.

For Prandtl–Meyer's flow

- the continuity equation;
- Euler's equation;
- Bernoulli's equation:

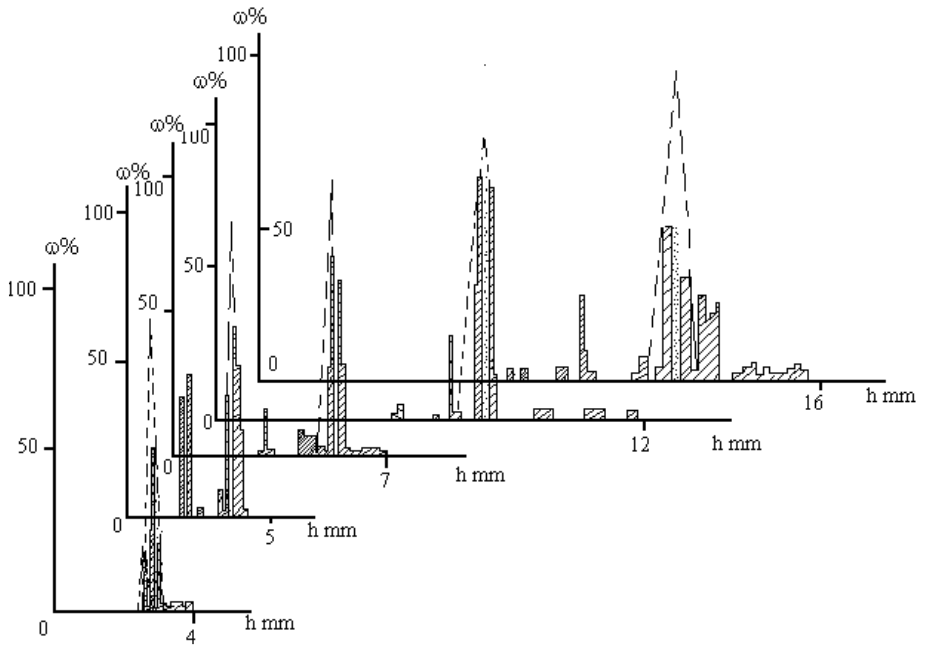


Fig. 4. Experimental distribution of the damage ($\omega$) as a function of the coordinate ($X$) in specimens of steel $C_T$ 3. $\equiv$ – rupture zone, i.e. complete fracture zone. The dotted lines are calculated by relation (3). $H$ is the thickness of specimens. $X = 0$ is the free surface.

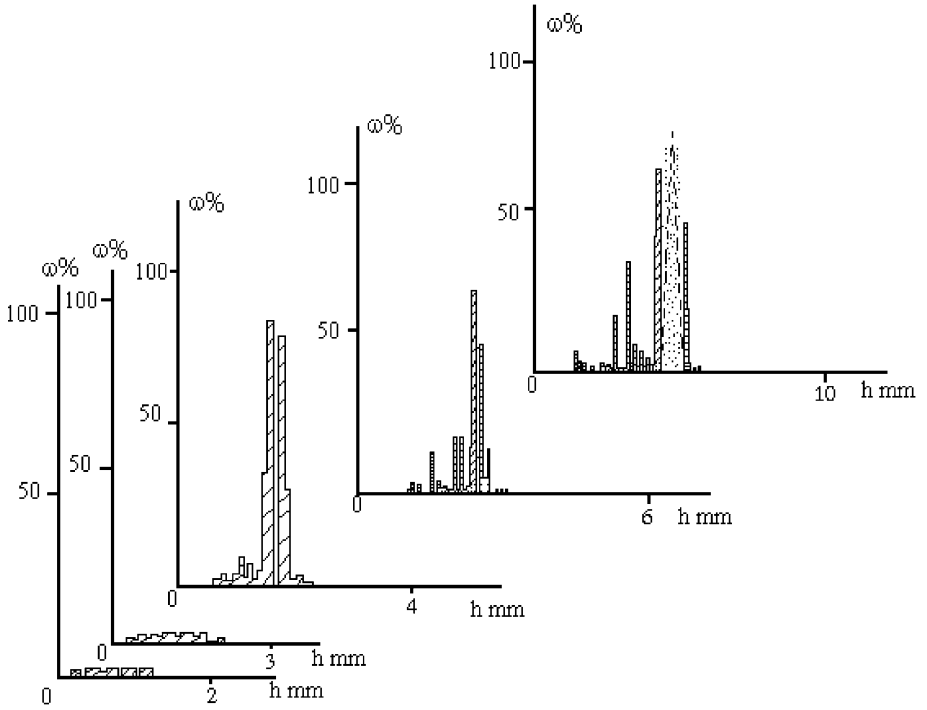


Fig. 5. $\omega(x)$ for aluminium alloy D16.

Table 2

| Materials | Experimental data | | | | Calculated data | | | | |
|---|---|---|---|---|---|---|---|---|---|
| | Thickness of sample $H$ (mm) | Thickness of spalled layer $\delta$ (mm) | Width of fracture zone (mm) | Width of complete fracture zone $\Delta$ (mm) | Width of range of waves interaction $(0 - X_0)$ (mm) | Tension time duration $t_\Sigma$ (μs) | $\partial P_*/\partial x$ (GPa/mm) | $\partial t/\partial x$ (μs/mm) | $t_{\text{expl}}$ (μs) |
| Steel $C_T3$ | 4 | 1.1 | 1.0 | 0.05 | 3.40 | 1.632 | 1.63 | −0.74 | 0.012 |
| | 5 | 1.4 | 0.9 | 0.15 | 3.73 | 1.60 | 1.40 | −0.72 | 0.01 |
| | 7 | 1.75 | 0.6 | 0.12 | 4.34 | 1.51 | 1.09 | −0.68 | 0.012 |
| | 12 | 3.5 | 0.8 | 0.20 | 5.39 | 1.15 | 0.76 | −0.63 | 0.02 |
| | 16 | 3.8 | 2.5 | 0.30 | 6.00 | 0.72 | 0.63 | −0.62 | 0.03 |
| Aluminium alloy D16 | 2 | – | – | – | | | | | |
| | 3 | – | – | – | | | | | |
| | 4 | 1.60 | 1.1 | 0.06 | 3.40 | 1.632 | 1.63 | −0.74 | 0.008 |
| | 6 | 1.90 | 1.40 | 0.16 | 4.08 | 1.57 | 1.22 | −0.69 | 0.014 |
| | 10 | 3.0 | 2.75 | 1.00 | 5.10 | 1.35 | 0.84 | −0.64 | 0.02 |

For the loaded material

- equations of mass and momentum conservation;
- equality equations of tangential velocity components.

The diagram ($P$–$\theta$) was plotted by means of these equations. The magnitudes of pressures and angles comprised 17.5 GPa and 2.5° for steel and 14.1 GPa and 4.5° for aluminium alloy (Rybakov, 1993a,b). The experimental results of Rybakov (1985) allowed us to find the value of specific mechanical pulse (momentum) for the explosive sheet charge of 2 mm thick. If the form of loading pulse is assumed to be triangular then the pulse duration is 0.798 μs. The finite thickness of sheet charge causes shock wave damping in specimen. The rarefaction wave from the free surface of detonation products reaches the shock wave in the specimen and decreases the pressure amplitude of the shock wave pulse, increasing at the same time the shock wave pulse duration. The shock-wave velocity drops. The trajectory of shock front becomes curvilinear (see 6 in Fig. 2). Then the experimental law obtained by Rybakov (1987) of shock wave attenuation is used

$$U = U_0[1 + 20(H/h_E)(1/\cos(\arcsin(C_0/D_E)]^{-0.27}, \tag{1}$$

here $u$ is the current value of specimen material particle velocity; $U_0$, the particle velocity on the contact boundary; $U_0 = 0.428$ km/s for steel and $U_0 = 0.8$ km/s for aluminium alloy D16; $H$, the specimen thickness; $h_E$, the explosive sheet charge thickness; $D_E$, the detonation velocity; $C$, the sound speed in the specimen material.

Decrease in particle velocity reduces the pressure amplitude. The pressure ($P$) and particle velocity ($u$) are related by the Renkin–Hugoniot ratio. The loading pulse duration $\tau$ has been increasing with the pressure amplitude decrease

$$p\tau = \text{const}. \tag{2}$$

The calculation of state parameters for the tensile stress region has been carried out in terms of acoustic approximation. When the oblique compression wave has approached the free surface of a specimen, two reflected waves go back into it (see e.g. Kolsky and Reider, 1973). The first is a tensile wave and the second is a shift wave. The shift wave propagates at velocity less than that of the tensile wave by a factor of two.

Therefore, further no consideration will be given to the shift wave. The interaction of shock wave and reflected rarefaction wave produces tensile pulses in each section parallel to the free surface (see Broberg, 1960). The amplitude of this tensile pulse increases with a distance increase from the free surface of a specimen whereas its duration decreases. Fig. 2 shows the tensile pulse for spall section. The amplitudes and duration of tensile pulses were calculated for each section parallel to the free surface and for all regions of shock waves and reflected rarefaction waves interaction located near the free surface. These calculations were made for steel and aluminium alloy. Variation of tension time and of tensile stresses is shown in Figs. 1 and 6. Some numerical results are presented in the Table 2. They are: the width of a zone of shock and rarefaction waves interaction, partial derivatives of the tensile stress and tension time with respect to the coordinate $x$ in this region: the time of impetuous explosive fracture.

## 5. Discussion

### 5.1. Damage distribution

Experimental data show that damage is distributed non-uniform along thickness of specimens (see Figs. 4 and 5). The damage is practically absent near free surface and near surface loaded. At least, it equals to one that is in unloaded specimens. Damage degree rises towards the spall-fracture zone. And magnitude of damage factor rises too. In the experiments described earlier, the load is constant. It is the same in each experiment. The changing of specimen's thickness, changes the parameters of state in spall-fracture zone. The nature of damage distribution changes too, which is presented in Figs. 4 and 5. Here we should make two remarks. Firstly, the separation of specimens into parts takes place at the damage factor of 60–80% and larger. No rupture is observed at value 30% taken by some authors (see e.g. Johnson, 1981; Akhmadieev, 1983; Kanel et al., 1984) as a criterion of complete fracture of specimens. Secondly, the cracks are sheet-shaped and parallel to the free surface as we can see from the comparison of damage-pictures on specimen cross-section parallel and perpendicular to the direction of detonation wave propagation. This result confirms that the assumptions made are correct. Namely, the acoustical model of spallation and estimation of state parameters in the fracture zone are true in this case.

### 5.2. Localization of fracture

It should be noted that the spall-fracture is localised in a certain narrow region near the free surface of the specimen. Needless to say that this zone can be observed only in the region of shock and rarefaction waves interactions. The width of interaction region is $(0–x_0)$. Experimentally it has been found that the discontinuity takes place exclusively in the region $(0–x_0)$. In particular, the values of damage factor $\omega$ in the region $(0–x_0)$ are greater than several tens of percent and are equal to the background values outside this region $(0–x_0)$. Furthermore, there is a narrow zone of width $\Delta$ within the region $(0–x_0)$ bounded by the coordinate $x$ on one side (on the right in Fig. 1) where the tension time equals the induction time $t_{\text{ind}}$ (Fig. 1). On the other side (on the left in Fig. 1), it is bounded by the coordinate $x$ where the tensile stress equals $P_{\text{conc}}$. In Fig. 1 the zone $\Delta$ is not shaded whereas the regions to the right and to the left of this zone are horizontally shaded. Within the region, there are magnitudes of tensile stress and tension time greater than those of thresholds, i.e. $t > t_{\text{ind}}$, $P > P_{\text{conc}}$. From experimental histograms in Figs. 4 and 5 the magnitudes of $t_{\text{ind}}$ and $P_{\text{conc}}$ are $t_{\text{ind}} = 1 \pm 0.2$ μs; $P_{\text{conc}} = 1 \pm 0.2$ Gpa.

The spallation was not experimentally found for aluminium alloy D16 specimens 2 and 3 mm thick. Dependencies of the tensile stress and tension time on co-ordinate also give $\Delta = 0$ for these specimens. The width of zone $\Delta$ is a finite magnitude for other samples and therefore the spallation takes place.

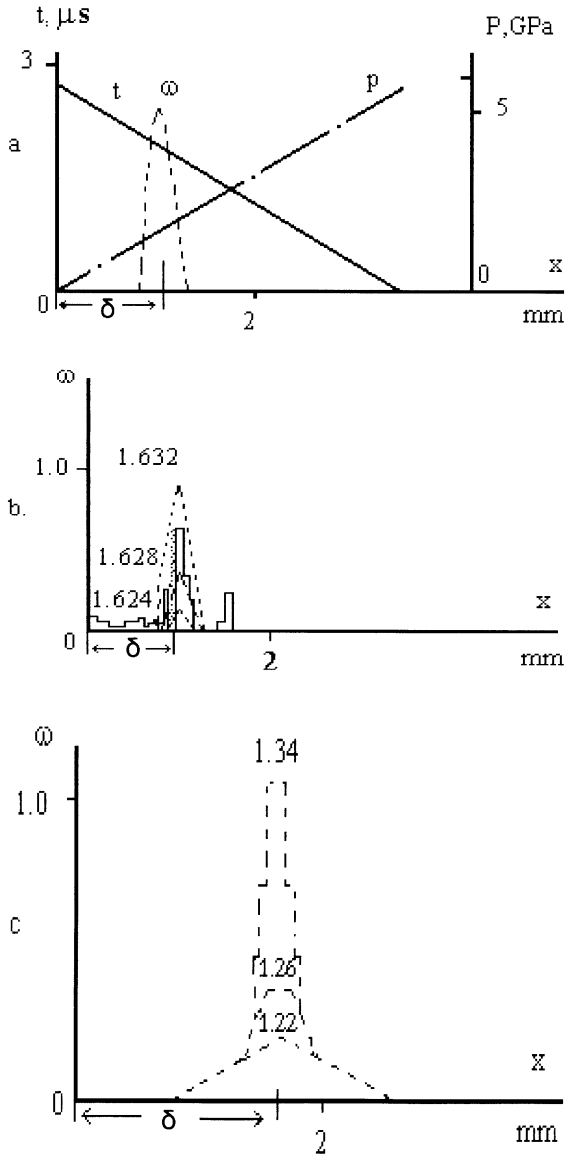


Fig. 6. Experimental and calculated results for aluminium specimen of thickness of 4 mm. (a) Calculated tension time ($t$) and tensile pressure ($P$) as the functions of the coordinate ($x$) in the region near the free surface. $\delta$ is the thickness of spalled layer. (b) damage versus specimen thickness. Half-tone histogram is experimental one; dotted lines are calculated by relation (3); $x = 0$ is the free surface. Numbers about curves indicate time in μs. (c) numerical data of Beliaev in the framework of her model.

### 5.3. Fracture behaviour

Experimental results of damage distribution and estimation of state parameters in the fracture zone permit to express hypothesis that spall-fracture process has all features of self-accelerating explosive reaction (Zeldovich et al., 1980), except localization. They are: (i) energy release due to fracture chain reaction; (ii) involving the products into reaction; (iii) induction time; (iv) very short subsequent time of

impetuous development and completion of fracture reaction. First two features have been widely admitted (among works on this subject see e.g. Beliaev et al., 1989). As for the remaining two features, we will further analyse them and make some general observations. Firstly, as the induction time $t_{ind}$ passes the concentration of reaction products, i.e. the magnitude of damage factor in our case, reaches the value which can be measured, that is, it has a value of 10% (Zeldovich et al., 1980).

Secondly, it is probable that the threshold concentration of reaction germes also exists. The tensile stress magnitude controls the concentration of germes of different kinds, fracture locations under spallation. Thus, there exists the tensile stress threshold $P_{conc}$. At magnitudes of tensile stress and tension time smaller than those of thresholds, no explosive fracture reaction takes place and the spallation is absent. This hypothesis would form a link to the approach taken by some authors (Curran et al., 1987; Grady, 1988; Eftis and Nemes, 1991). Under fracture the magnitudes of state parameters are continuously varied in the fracture zone. On the one hand, the stress must decrease as the medium fragmentation takes place. It might also be expected that the temperature increases whereas the internal energy decreases. On the other hand, stress will increase because of the energy release resulting from the fracture. Thus, there exist two competitive processes which should be necessarily considered to correctly describe the state of fracturing media in a proper and correct way.

### 5.4. Time-durations relation

The experimental results (Figs. 4 and 5) have been described earlier in Rybakov (1993a,b) by the semiempirical formula

$$\omega = \omega^* \exp\left[P/P_*(C \ln(B + At)\right]. \tag{3}$$

Here $\omega^*$ equals 1 for the first spall; $A$, $B$, $C$, $P_*$ are determined by characteristics of the sample material and by geometry of the experimental device, i.e. by loading conditions parameters. Formula (3) gives the following expression for the thickness of a spalled 1ayer:

$$\delta = 0,57H\xi^{-0.84}\mathrm{e}^{0.048\xi}. \tag{4}$$

Here, as before $\delta$, $h$, $H$ are

$$\xi = H/h.$$

Expression (4) is valid for high explosive sheet charges and allows us to obtain results confirmed by the experimental data of Rybakov (1993a,b). Expression (3) was used in Rybakov (1993a,b) to describe the final damage distribution. Later, it has been shown that it is applicable to describe kinetics (see e.g. Rybakov and Rybakov, 1995; Rybakov, 1996a,b). Figs. 6 and 7 show the curves $\omega(x)$ for different times calculated by expression (3). The time-duration of fracture reaction explosive development, $t_{expl}$, is assumed to be equal to the time period from $\omega = 0.1$–$1.0$. In this case, the time intervals for tensile action $t_\Sigma$ and fracture explosive development $t_{expl}$ are also given in the Table 2. It is seen that the total interval equals the sum of $t_{ind}$ and $t_{expl}$ and that $t_\Sigma \approx t_{ind}$, thus $t_{expl}$ is too short comprising only $10^{-8}$–$10^{-7}$ s. This result has been also confirmed by the numerical analysis performed by Beliaev et al. (1989) for aluminium alloy D16 in the framework of the model for non-equilibrium static thermodynamics. The results obtained by him and by us are shown in Fig. 6 for the aluminium specimen of 4 mm thick. Here, one may observe the quantitative and qualitative conformity. This fact confirms correctness of assumption that acoustical model is true in this case. The velocity of fracture reaction increases with time and reaches a significant magnitude after $t_{ind}$. Formula (3) demonstrates further growth of the velocity at least by an order of magnitude for $t_{expl}$. The ultimate value of fracture velocity is the sound speed magnitude. Let us assume that the above is valid for $\omega = 1$, i.e. $V_{fr} \leqslant 10^4$ m/s, and for $\omega = 0.1$, $V_{fv} \leqslant 10^3$ m/s. Therefore, the width of complete fracture zone

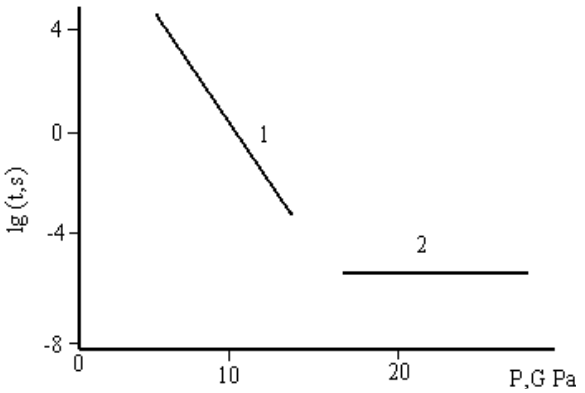


Fig. 7. Time dependence of tensile stress for polymethilmethacrilate from work of Evseenko et al. 1 – statically branch. 2 – dynamical branch.

equals $10^4$ m/s $\cdot$ ($10^{-8}$–$10^{-7}$) s = $10^{-4}$–$10^{-3}$ m, and that of partial fracture zone is $10^3$ m/s $\cdot$ $10^{-6}$ s = $10^{-3}$ m. These estimations are supported by the experimental data from the Table 2.

Now we should make some remarks. The extreme short times of fracture development permit us to note that under spallation there is no magistral crack which propagates along the complete fracture zone, but not across it. The fracture takes place at the same time in all points of any particular plane parallel to the free surface. In other words, the fracture simultaneously occurs over the total volume of complete fracture zone. In particular, under sliding detonation loading, the fracture appears simultaneously along the line parallel to the shock front. The presence of ultimate induction time $t_{ind} \approx 10^{-7}$–$10^{-6}$ s gives good grounds to say that the time dependence of fracture stress does exist at times smaller than a fraction of a microsecond (Fig. 7). The duration of tensile stresses amounts approximately half of the shock wave duration which in turn has the magnitude from a few tenths of microseconds to several microseconds for waves induced in laboratory conditions. It is the time interval where that the part of dynamical branch of longevity caused by the mechanism of spall fracture will exist. As before, it is the time interval where the spall formation and the part of dynamical branch of longevity have been experimentally found. In particular, this phenomenon has been marked by Evseenko et al. (1977) and in Rybakov (1985,1996a,b). As soon as the shock wave duration becomes smaller than the induction time, the spallation as well as the part of dynamical branch of longevity dictated by spall-fracture will not occur. In the other words, it would make no sense to say about, the presence of dynamical branch of longevity caused by spall-fracture at times smaller than $10^{-7}$ s. Beliaev et al. (1989) have arrived at the same conclusion by a different way. However, it is quite possible that the dynamical branch of longevity at times smaller than $10^{-7}$ s might be released using other techniques.

## 6. Conclusion

The main results of this paper are listed below:

1. Experimental systematical study of damage distribution along thickness of specimens for specimens of different thickness under the same load in each experiment has been fulfilled.
2. On the basis of the simplest acoustical model and hydrodynamic description of wave-flows, an engineering model for predicting the extent of spall in impulsively loaded specimens has been proposed.
3. This model involving the analogy of the spall process to the kinetics of an explosive reaction is totally applicable to the induction-time model.

## References

Akhmadieev, N.H., 1983. Investigation of spall damage under shock deformation. Model of damage medium. J. Appl. Mech. Tech. Phys. 4, 158–167 (in Russian).

Altshuler, L.V., Novicov, S.A., Divnov, I.I., 1966. Connection of critical damage stresses with damage time under explosive fracture of metals. Sov. Phys. Doklady 166, 67–70.

Beliaev, V.V., Naimark, O.B., 1989. The kinetics of microcracks accumulation and stages of failure in shock waves. Phys. Combust. & Expl. 24, 115–123 (in Russian).

Broberg, K.B., 1960. Some aspects of the mechanism of scabbing in stress wave propagation in materials. Proc. Int. Symp. Stress Waves Mat. Interscience, pp. 228–246.

Curran, D.R., Seaman, L., Shockey, 1987. Dynamic failure of solids. Phys. Rep. 147, 253–388.

Eftis, J., Nemes, J.A., 1991. Constitutive modelling of spall fracture. Arch. of Mech. 43, 399–435.

Evseenko, E.P., Zilberbrand, E.L., Zlatin, N.A., Pugachov, G.S., 1977. Dynamical branch of time dependence strength of polymethilmethacrilate. Sov. Phys.-JETF Lett. 3 (9), 684–687 (in Russian).

Grady, D.E., 1988. The spall strength of condensed matter. J. Mech. Phys. Solids 36, 353–384.

Johnson, J.N., 1981. Dynamic fracture and spallation in ductile solids. J. Appl. Phys. 52, 2812–2825.

Kanel, G.J., Razorionov, S.V., Fortov, V.B., 1984. Kinetics of fracture of aluminium alloy AMG6M at spall-conditions. J. Appl. Mech. Tech. Phys. 4, 60–64 (in Russian).

Kanel, G.I., Razorionov, S.V., Utkin, A.V., Fortov, V.E., 1999. Shock-Wave Phenomena in Condensed Media. Moscow, Ianus-K, p. 408.

Kolsky, G., Reider, D., 1973. Stress wave and fracture. Fracture. Moscow, Mir, pp. 570–608.

Novikov, S.A., 1985. Strength under quasistatic and shock-wave loading. Phys. Combust. Expl. 21, 77–85 (in Russian).

Novicov, S.A., 1999. The fracture of materials under intense shock loads. Soros Educ. J. 8, 16–21.

Rinehart, J.S., Pearson, J., 1954. Behaviour of Metals Under Impulsive Loads. ASM, Cleveland, Ohio.

Rybakov, A.P., 1985. Shock Waves in Condensed Media. Part 1. Daugavpils, University Press.

Rybakov, A.P., 1987. Shock Waves in Condensed Media. Part 2. Daugavpils, University Press, (in Russian).

Rybakov, A.P., 1991. Plane flow of detonation products. Proceed. Latv. Acad. Sci. 11, 102–110.

Rybakov, A.P., 1993a. Spall damage of two metals under influence of sliding detonation. Latv. J. Phys. Tech. Sci. 3, 26–33.

Rybakov, A.P., 1993b. Hydrodynamics of Oblique Waves in Condensed Media. Daugavpills, University Press.

Rybakov, A.P., Rybakov, I.A., 1993. Hydrodynamics of oblique waves in condensed media. Latv. J. Phys. Tech. Sci. 6, 21–33.

Rybakov, A.P., Rybakov, I.A., 1995. Spall damage kinetics of metals. Latv. J. Phys. Tech. Sci. 1, 3–9 (in Russian).

Rybakov, A.P., 1996a. Spall Fracture Mechanics. Perm, Military Institute of Missiles and Rockets (in Russian).

Rybakov, A.P., 1996b. Response of Condensed Media to Short-Duration Loads. Perm, ICMM Press.

Zeldovich, Ja.B., Barenblatt, G.J., Librovich, V.B., Makhviladze, G.M., 1980. Mathematical theory of Combustion and Explosion. Nauka, Moscow (in Russian).

Zlatin, N.A., Mochalov, S.M., Pugachov, G.S., Bragov, A.M., 1984. Time regularities of fracture-metals process under intensive loads. Sov. Phys. Solid Physics 16, 1752–1755 (in Russian).